Check for updates

Poly(lactic acid) stereocomplex microspheres as thermally tolerant optical resonators†

Suharman, [ID] [a,b] Wey Yih Heah,[c] Hiroshi Yamagishi [ID] [a,c] and Yohei Yamamoto [ID] *[a,c]

Thermally tolerant polymer optical resonators are fabricated from a stereocomplex of poly(L-lactic acid) and poly(D-lactic acid) through the oil-in-water miniemulsion method. The thermal stability of the microspheres of the stereocomplex poly(lactic acid) (SC-PLA) is superior to that of the homochiral poly(lactic acid) (HC-PLA). As a result of the high thermal stability, the optical resonator properties of the SC-PLA microspheres are preserved at an elevated temperature of up to 230 °C, which is 70 °C higher than that of microspheres formed from HC-PLA.

Poly(lactic acid) (PLA) is a synthetic polyester made from lactic acid.[1–4] Due to its biodegradable, biocompatible, and nontoxic properties, PLA is widely used in biomedical applications,[5–7] drug transportation,[8] textile,[9] and packaging.[10,11] PLA has three types of stereoisomers: poly(L-lactide acid) (PLLA), poly(D-lactide acid) (PDLA), and their atactic polymer, poly(DL-lactic acid) (PDLLA).[12] The homopolymers of PLLA and PDLA form semicrystalline aggregates with a melting temperature of around 170 °C, while the atactic PDLLA copolymer forms an amorphous aggregate with a lower melting temperature.[13]

One of the drawbacks of PLA is that its thermal stability is not so high due to its low crystallinity, which limits its use in optical and electronic applications.[14] Some techniques have been applied to enhance the thermal stability of PLA by adding a nucleating agent,[15–18] physical modification through fibre reinforcement,[19,20] the addition of inorganic particles,[21] chemical modification,[22] and blending it with a material with high T_g and high heat resistance.[23,24] In particular, stereocom-

plexation by mixing PLLA and PDLA has received much attention due to its enhanced thermal and mechanical properties.[25,26] A mixture of PLLA and PDLA, prepared from its molten state or solution state, induces the formation of stereocomplex PLA (SC-PLA) driven by the intensive intermolecular hydrogen (H)-bonding and dipole–dipole interactions between PLLA and PDLA (Fig. 1).[27–29] Compared with homochiral PLA (HC-PLA), SC-PLA has a melting temperature (T_m) of around 230 °C, which is higher than that of pure HC-PLA (~170 °C), since the intermolecular H-bonding interaction between PLLA and PDLA chains increases the rigidity of the PLA chains.[30–35]

Optical resonators confine light in a small volume that interferes with itself and shows up sharp resonant optical signals.[36] Typical optical resonators are Fabry–Pérot (F–P) resonators and whispering gallery mode (WGM) resonators.[37] For F–P resonators, light is confined between counter mirrors or crystalline facets.[38] On the other hand, WGM resonators confine light circularly by total internal reflection (TIR) at the interface between the inner and outer media with different refractive indices. Typical WGM resonators have shapes of
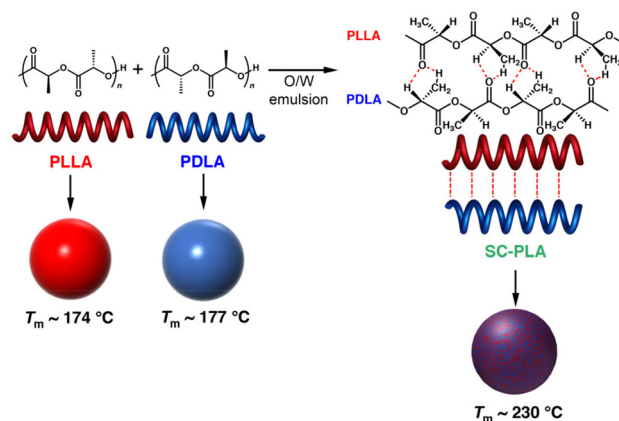
[a]Department of Material Innovation, Graduate School of Pure and Applied Science, University of Tsukuba, 1-1-1 Tennodai, Tsukuba, Ibaraki, 305-8573, Japan
[b]Department of Chemistry, Faculty of Mathematics and Natural Science, Universitas Sumatera Utara, Jl. Dr. T. Mansur No. 9, Padang Bulan, Medan Baru, Medan, Sumatera Utara 20222, Indonesia
[c]Department of Material Science, Institute of Pure and Applied Science, University of Tsukuba, 1-1-1 Tennodai, Tsukuba, Ibaraki, 305-8573, Japan.
E-mail: yamamoto@ims.tsukuba.ac.jp
†Electronic supplementary information (ESI) available. See DOI: https://doi.org/10.1039/d3nr05318k

Fig. 1 Schematic illustration of the fabrication of microspheres from HC- and SC-PLA by the O/W miniemulsion method.

spheres, rings, polyhedra *etc.*[39] WGM is highly sensitive to the surface morphology because a rough surface tends to scatter light, which reduces the light confinement efficiency in the resonator.[40] Therefore, a highly smooth surface is one of the important factors for high quality factor (Q) microresonators. The sharp PL peaks from the resonators are utilized for highly sensitive chemical and biosensing applications by monitoring the peak shift.[41,42]

In this work, we investigated the optical resonator properties of the microspheres formed from PLAs. The whispering gallery mode (WGM) microresonators are fabricated from a blend of PLLA and PDLA through the oil-in-water (O/W) miniemulsion method. We expect that the microresonators formed from SC-PLA have better thermal stability than the microresonators formed from pure HC-PLA. We found that the WGM resonators from SC-PLA are much more stable even at 230 °C in comparison with those from HC-PLA (~170 °C).

Microspheres of HC-PLA composed of PLLA (the number average molecular weight, M_n = 40 kg mol^{-1}) or PDLA (M_n = 90 kg mol^{-1}) were prepared by the O/W miniemulsion method. Similarly, microspheres of SC-PLA composed of a blend of PLLA and PDLA were fabricated with mixing ratios of PLLA to PDLA (L/D) of 9/1, 7/3, 5/5, 3/7, and 1/9. The miniemulsion method is chosen because of the efficient formation of SC-PLA with a high reaction rate compared to other methods such as solution blending, supercritical fluid mixing, and melted blending.[32,43] During the emulsification and subsequent solvent evaporation processes, PLLA and PDLA form a stereocomplex.

Fig. 2 shows scanning electron microscopy (SEM) images of the resultant microspheres formed from HC- and SC-PLA. All the microspheres have high sphericity but have different surface morphologies. The microspheres of HC-PLA with an L/D ratio of 10/0 containing only PLLA (Fig. 2a and b) and SC-PLA with L/D ratios of 9/1 and 7/3 (Fig. 2c and d, respectively) have rather smooth surfaces with the values of the root-mean-square (RMS) roughness between 4 and 5 (for details on the calculation of the RMS roughness, see the ESI†). The surface of the microsphere becomes rough with the increase of the content of PDLA with L/D ratios of 5/5, 3/7 and 1/9 with the values of the RMS roughness being 6.23, 11.5, and 14.6, respectively (Fig. 2e–g). As for the microparticles made from only PDLA (L/D = 0/10), the surface morphology is quite rough with an RMS roughness value as large as 46.3 (Fig. 2h). The difference in the surface morphologies of the microspheres from PLLA and PDLA is possibly due to the difference in the molecular weights of these polymers, which causes the different crystallinity of the microspheres.[44]

We investigated the change in the morphology of the microsphere by heating. As shown in Fig. S1,† the microspheres of HC-PLA (L/D = 10/0 and 0/10) melt when heated at 200 °C for 2 s. However, microspheres of SC-PLA with L/D ratios of 9/1, 7/3, 5/5, 3/7, and 1/9 keep their spherical morphologies after being heated at 200 °C, indicating that the thermal stability of PLA is remarkably improved by SC formation. Even for a microsphere with an L/D ratio of 9/1, where the composition of HC crystal-

Fig. 2 SEM micrographs of HC-PLA and SC-PLA microspheres prepared by the O/W miniemulsion method with different L/D ratios of 10/0 (a and b), 9/1 (c), 7/3 (d), 5/5 (e), 3/7 (f), 1/9 (g), and 0/10 (h). The graphs on the right in (b–h) show the profiles of the difference in the gray values *versus* the distance (d) at the cross section of the microspheres shown as yellow-dotted lines in the corresponding micrographs.

lites is greater than that of SC crystallites, the microsphere preserves its spherical morphology upon heating at 200 °C.

The thermal stability of HC- and SC-PLA microspheres was investigated in more detail by differential scanning calorimetry (DSC). Fig. 3 shows the DSC thermograms (first heating) of the HC and SC crystallites with different mixing ratios (L/D = 10/0, 9/1, 7/3, 5/5, 3/7, 1/9, and 0/10). Several characteristic endo-/exothermic peaks were observed: endothermic peaks at 60–70 °C due to the glass transition (T_g), exothermic peaks at 90–110 °C due to the crystallization (T_c), and endothermic
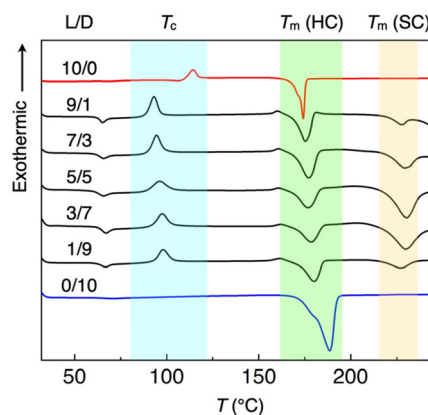

Fig. 3 DSC traces of HC- and SC-PLA with different L/D ratios.

peaks at >170 °C due to the melting of the HC and SC crystallites. For HC-PLA (L/D = 10/0 and 0/10), T_m appears at 174 and 177 °C, respectively. In contrast, for SC-PLA, another peak appeared at 227–230 °C, which is attributed to the T_m of the SC crystallites.[25] These results indicate that blending PLLA and PDLA forms both SC and HC domains.

The thermal properties of HC- and SC-PLA are summarized in Table 1. From the peak area of T_m in the DSC thermograms, the melting enthalpies (ΔH_m) of the HC and SC crystallites are determined. By changing the L/D ratio from 10/0 to 5/5, the ΔH_m of HC-PLA (ΔH_{HC}) decreases from 54 to 24 J g^{-1} and then increases to 71 J g^{-1} by further changing the L/D ratio to 0/10. Concomitantly, the ΔH_m of SC-PLA (ΔH_{SC}) significantly increases from 9 to 45 J g^{-1} and then decreases to 15 J g^{-1} upon increasing the PDLA content. The ΔH_{HC} and ΔH_{SC} values show minimum and maximum at an L/D ratio of 5/5, indicating that PLA mostly forms SC domains in the 5/5 mixture of PLLA and PDLA.[45] Moreover, the decomposition temperatures (T_{dec}) of both HC- and SC-PLA were determined using thermogravimetry differential thermal analysis (TG/DTA, Fig. S2†). For pure HC-PLLA, T_{dec} was at around 280 °C. As the ratio of PDLA to PLLA increased, T_{dec} increased and reached 337 °C for an L/D ratio of 1/9. For pure HC-PDLA, T_{dec} reached 354 °C. Therefore, T_{dec} is mainly affected by the M_n of PLA, where a large M_n has a high T_{dec}. However, the TGA profiles of SC-PLA show a single decomposition step, indicating that the stereocomplex state is not only a simple mixture of PLLA and PDLA but also has a strong interaction between PLLA and PDLA *via* H-bonding (Fig. 1).

To understand the crystalline states of HC- and SC-PLA, powder X-ray diffraction (PXRD) measurements were conducted. As shown in Fig. 4a, powder samples of HC-PLA with L/D ratios of 10/0 and 0/10 show diffraction peaks at 2θ = 14.9, 16.7, 19.1, and 22.4°, which are assigned to the (010), (110)/(200), (203), (015) planes of the HC crystallites, respectively. In comparison, powder samples with the blend of PDLA and PLLA exhibit three additional diffraction peaks at 12.0, 20.8, and 24.1°, which are assigned to the (110), (300)/(030), (220) planes of the SC crystallites, respectively.[25,26,46] For the sample with an L/D ratio of 5/5, diffractions from the HC crystallites mostly disappeared. The percentages of the crystallites (X_c) of HC- and SC-PLA are calculated from the intensity ratios of the diffraction peaks of the HC and SC crystallites to the entire

Fig. 4 (a) PXRD patterns of HC- and SC-PLA microspheres. (b) The relative degree of crystallinity (X_c) of the HC and SC crystallites. (c–f) Relative degree of X_c versus temperature in the range of 25 to 220 °C for HC and SC crystallites of PLA with L/D ratios of 10/0 (c), 9/1 (d), 7/3 (e), and 5/5 (f).

diffraction. The X_c value of HC decreases when the L/D ratio changes from 10/0 to 5/5 and then increases when the L/D ratio reaches 0/10 (Fig. 4b, blue). Conversely, the X_c value of SC increases (decreases) when that of HC decreases (increases) (Fig. 4b, red).

PXRD measurements were further conducted by elevating the temperature from 25 to 220 °C (Fig. S3†). For samples with L/D ratios of 10/0, 1/9, 9/1, and 0/10, the diffraction peaks of the HC crystallites disappear at 200 °C due to the melting of the HC crystallites. For samples with L/D ratios of 7/3, 5/5, and 3/7, small diffraction peaks from the HC crystallites remain at 200 °C, but they completely disappear at 220 °C. In contrast, the diffraction peaks of the SC crystallites remain even at 220 °C. These results are consistent with the DSC results, where the T_m of HC-PLA is around 180 °C while that of SC-PLA is around 230 °C.[47] Fig. 4c–f plot the X_c values *versus* temperature for the HC and SC crystallites. The X_c value of the HC crystallites abruptly drops at 200 °C, and simultaneously, the X_c value of the SC crystallites increases at 200 °C. These results indicate that the melting of the HC domain subsequently induces the formation of the SC domains.

The microspherical structure with a smooth surface is advantageous for use as a WGM optical resonator.[48–50] As schematically drawn in Fig. 5a, photoluminescence (PL) gener-

Table 1 Summary of the thermal behaviour of HC- and SC-PLA microspheres with different L/D ratios

Sample	T_g (°C)	T_c (°C)	T_m, HC (°C)	T_m, SC (°C)	ΔH_{HC} (J g^{-1})	ΔH_{SC} (J g^{-1})
HC-PLA 10/0	—	109	174	—	54	—
SC-PLA 9/1	65	93	176	227	47	9
SC-PLA 7/3	66	95	175	229	24	42
SC-PLA 5/5	66	96	177	230	24	45
SC-PLA 3/7	67	98	177	229	24	41
SC-PLA 1/9	67	98	179	227	33	15
HC-PLA 0/10	—	—	177	—	71	—

ated at the surface of the polymer microsphere is confined *via* total internal reflection at the medium/air interface and interferes with itself showing up sharp and periodic resonant PL lines.[51–58] To investigate the optical resonator properties of the PLA microspheres, HC- and SC-PLA microspheres are doped with a fluorescent dye, zinc(II) tetraphenylporphyrin (ZnTPP), with T_m (~350 °C) higher than that of PLA. The ZnTPP-doped HC- or SC-PLA microspheres are dispersed on a quartz substrate by a spin coating method. PL spectra of a single HC- and SC-PLA microsphere are recorded upon focused laser excitation with a 405 nm continuous wave (cw) laser to a single microsphere.[59–63] At 30 °C, the PL spectra of a HC-PLA microsphere show periodic PL lines, attributed to WGMs (Fig. 5b). As shown in Fig. S4,† these resonant peaks are assigned to transverse electric (TE) and transverse magnetic (TM) modes. The free spectral range (FSR) of four microspheres with different sizes is plotted in Fig. S5.† The FSR is measured using the following equation:

$$FSR = (\lambda^2/n\pi) \cdot (1/d),$$

which indicates that the PLA microspheres certainly act as an optical resonator.[64] The clear WGM peaks in the PL spectra are maintained upon thermal heating of the microspheres up to 160 °C (see Fig. S6a† for more details). By further heating at

170 °C, these WGM PL peaks disappear due to the melting of HC-PLA that causes the deformation of the microspherical morphology.

The optical resonator properties are observed for the microspheres of SC-PLA with L/D ratios of 9/1 and 7/3 (Fig. 5c and d, respectively). Intriguingly, the thermal stability of the microresonator is preserved upon thermal heating up to 230 °C. The WGM PL peaks disappear by heating the microspheres at 240 °C (see Fig. S6b and c† for more details). In Fig. 5e, temperature dependencies of the WGM peak intensity, normalized by the PL intensity of the background unconfined PL, are plotted. It is obvious that the thermal stability of the optical resonator is higher by ~70 °C for the microspheres of SC-PLA with L/D ratios of 9/1 and 7/3 than that of the HC-PLA microspheres (L/D = 10/0). It is worth noting that the phase transition of PLA affects the shape of PL spectra, possibly caused by the change in the aggregation manner of ZnTPP in the PLA microspheres. We confirm that the ratio of the PL intensities at 603 and 643 nm (I_{603}/I_{643}) from a cast film of the PLA microspheres varies at the phase transition temperature (Fig. S7†).

To gain insight into the resonant properties in more detail, the Q factor, defined as the wavelength of the resonant peaks divided by their full width at half maximum (FWHM), is evaluated.[65] Fig. 5f plots the Q factor of the PL peaks *versus* the heating temperature. The Q factor gradually increases upon heating, possibly due to the improvement of the surface roughness. However, phase transition causes the loss of the Q factor caused by the scattering of the confined light by the crystalline domains. For example, the Q factor of the HC-PLA microsphere (L/D = 10/0) dropped from 500 to 360 at 110 °C, where phase transition occurs from glass to the crystalline state. A further drop in the Q factor occurs at 170 °C, where melting of the HC-PLA microsphere takes place with the collapse of its microspherical morphology. In the case of SC-PLA with L/D ratios of 9/1 and 7/3, the Q factor drops once at ~200 °C, where HC-PLA crystallites melt and SC-PLA crystallites form, and finally drops off at 240 °C, at which the SC-PLA completely melts.

For comparison, SC-PLA microspheres with L/D ratios of 5/5, 3/7, and 1/9 display quite poor WGM PL (Fig. S8†), because the surface morphology of the microspheres is rather rough with the RMS roughness greater than 6 (Fig. 2). The light confinement is sensitive to the surface roughness, where the rough surface causes a scattering of the confined light, leading to the loss of the optical resonator properties.[65] Similarly, HC-PLA microspheres from PDLA (L/D = 0/10) do not show WGM PL due to the ill-defined spherical morphology (Fig. S8†).

In conclusion, we successfully prepared thermally tolerant optical resonators from stereocomplex crystallites of PLA formed by blending PLLA and PDLA through the oil-in-water miniemulsion method. The SC-PLA microspheres exhibit higher thermal stability in comparison with the HC-PLA microspheres, where the melting temperature of SC-PLA is more than 50 °C higher than that of HC-PLA. The relative degree of crystallinity of SC-PLA is maximum when the content of PLLA and PDLA is 5/5, as evaluated by PXRD studies. The tempera-

Fig. 5 (a) Schematic representation of the light confinement and WGM PL. (b–d) PL spectra of a single PLA microsphere after being annealed for 2 s upon photoexcitation at 405 nm with a cw laser. (e) Plots of the normalized PL intensity of the microspheres with L/D = 10/0, 9/1, and 7/3 *versus* annealing temperature. (f) Plots of the Q factor of the microspheres with L/D = 10/0, 9/1, and 7/3 *versus* annealing temperature.

ture-dependent PXRD results clearly show that PLAs maintain the stereocomplex structure even when the temperature reaches 220 °C. The temperature-dependent μ-PL spectra show that the SC-PLA resonators exhibit higher thermal tolerance in comparison with the HC-PLA resonators, where the WGM resonance properties of SC-PLA are preserved even at 230 °C. This work demonstrates a powerful strategy of stereocomplex formation toward thermally tolerant bio-related materials for optical applications.

Conflicts of interest

There are no conflicts to declare.

Acknowledgements

References

1 A. P. Dove, Controlled ring-opening polymerisation of cyclic esters: Polymer blocks in self-assembled nanostructures, *Chem. Commun.*, 2008, **48**, 6446–6470.

2 Y. Baimark, W. Rungseesantivanon and N. Prakymoramas, Preparation of stereocomplex-polylactide powder by precipitation method for potential use as nucleating agents in fully-biodegradable poly(L-lactide) composites, *Mater. Today Commun.*, 2022, **33**, 1–8.

3 S. Inkinen, M. Stolt and A. Södergård, Readily controllable step-growth polymerization method for poly(lactic acid) copolymers having a high glass transition temperature, *Biomacromolecules*, 2010, **11**, 1196–1201.

4 D. A. S. Marques, S. Jarmelo, C. M. S. G. Baptista and M. H. Gil, Poly(lactic acid) synthesis in solution polymerization, *Macromol. Symp.*, 2010, **296**, 63–71.

5 S. Zhang, D. Yan, L. Zhao and J. Lin, Composite fibrous membrane comprising PLA and PCL fibers for biomedical application, *Compos. Commun.*, 2022, **34**, 101268.

6 T. A. M. Valente, D. M. Silva, P. S. Gomes, M. H. Fernandes, J. D. Santos and V. Sencadas, Effect of sterilization methods on electrospun poly(lactic acid) (PLA) fiber alignment for biomedical applications, *ACS Appl. Mater. Interfaces*, 2016, **8**, 3241–3249.

7 M. Ekinci, C. C. Dos Santos, L. M. R. Alencar, H. Akbaba, R. Santos-Oliveira and D. Ilem-Ozdemir, Atezolizumab-Conjugated Poly(lactic acid)/Poly(vinyl alcohol) Nanoparticles as Pharmaceutical Part Candidates for Radiopharmaceuticals, *ACS Omega*, 2022, **7**, 47956–47966.

8 E. Ibrahim, K. Taylor, S. Ahmed, A. Mahmud and K. Lozana, Centrifugally spun poly(D,L-lactic acid)-alginate composite microbeads for drug delivery and tissue engineering, *Int. J. Biol. Macromol.*, 2023, **237**, 1–14.

9 S. Padee, S. Thumsorn, J. W. On, P. Surin, C. Apawet, T. Chaichalermwong, N. Kaabbuathong, T. O-Charoen and N. Srisawat, Preparation of poly(lactic acid) and poly(trimethylene terephthalate) blend fibers for textile application, *Energy Procedia*, 2013, **34**, 534–541.

10 E. Bianchi, G. Guidotti, M. Soccio, V. Siracusa, M. Gazzano, E. Salatelli and N. Lotti, Biobased and Compostable Multiblock Copolymer of Poly(l-lactic acid) Containing 2,5-Furandicarboxylic Acid for Sustainable Food Packaging: The Role of Parent Homopolymers in the Composting Kinetics and Mechanism, *Biomacromolecules*, 2023, **24**, 2356–2368.

11 J. Jacob, V. Robert, R. B. Valapa, S. Kuriakose, S. Thomas and S. Loganathan, Poly(lactic acid)/Polyethylenimine Functionalized Mesoporous Silica Biocomposite Films for Food Packaging, *ACS Appl. Polym. Mater.*, 2022, **4**, 4632–4642.

12 G. Liu, X. Zhang and D. Wang, Tailoring crystallization: Towards high-performance poly (lactic acid), *Adv. Mater.*, 2014, **26**, 6905–6911.

13 T. R. Cooper and R. F. Storey, Poly(lactic acid) and chain-extended poly(lactic acid)-polyurethane functionalized with pendent carboxylic acid groups, *Macromolecules*, 2008, **41**, 655–662.

14 G. Mattana, D. Briand, A. Marette, A. V. Quintero and N. F. D. Rooij, Polylactic acid as a biodegradable material for all-solution-processed organic electronic devices, *Org. Electron.*, 2015, **17**, 77–86.

15 H. Zhao, Y. Bian, M. Xu, C. Han, Y. Li, Q. Dong and L. Dong, Enhancing the crystallization of poly(L-lactide) using a montmorillonitic substrate favoring nucleation, *CrystEngComm*, 2014, **16**, 3896–3905.

16 M. Aouay, A. Magnin, J. L. Putaux and S. Boufi, Enhancing mechanical and thermal properties of plasticized poly-L-(lactic acid) by incorporating aminated-cellulose nanocrystals, *Ind. Crops Prod.*, 2023, **202**, 1–10.

17 X. Zhang, B. Yang, B. Fan, H. Sun and H. Zhang, Enhanced Nonisothermal Crystallization and Heat Resistance of Poly (l -lactic acid) by d -Sorbitol as a Homogeneous Nucleating Agent, *ACS Macro Lett.*, 2021, **10**, 154–160.

18 Y. Baimark, P. Srihanam, Y. Srisuwan and T. Phromsopha, Enhancement in Crystallizability of Poly(L-Lactide) Using Stereocomplex-Polylactide Powder as a Nucleating Agent, *Polymers*, 2022, **14**, 1–14.

19 S. Kadea, T. Kittikorn, R. Chollakup, R. Hedthong, S. Chumprasert, N. Khanoonkon, S. Witayakran and P. Chatakanonda, Influences of epoxidized natural rubber and fiber modification on injection molded-pulp/poly (lactic acid) biocomposites: Analysis of mechanical-thermal and weathering stability, *Ind. Crops Prod.*, 2023, **201**, 1–10.

20 J. Feng, Y. Sun, P. Song, W. Lei, Q. Wu, L. Liu, Y. Yu and H. Wang, Fire-Resistant, Strong, and Green Polymer

Nanocomposites Based on Poly(lactic acid) and Core-Shell Nanofibrous Flame Retardants, *ACS Sustainable Chem. Eng.*, 2017, **5**, 7894–7904.

21 Y. Li, L. Zhao, C. Han and L. Xiao, Thermal and mechanical properties of stereocomplex polylactide enhanced by nanosilica, *Colloid Polym. Sci.*, 2021, **299**, 1161–1172.

22 M. Tesfaye, R. Patwa, P. Dhar and V. Katiyar, Nanosilk-grafted poly(lactic acid) films: Influence of cross-linking on rheology and thermal stability, *ACS Omega*, 2017, **2**, 7071–7084.

23 H. Tsuji, S. Sato, N. Masaki, Y. Arakawa, Y. Yoshizaki, A. Kuzuya and Y. Ohya, Thermal properties and degradation of enantiomeric copolyesteramides poly(lactic acid-co-alanine)s, *Polym. Degrad. Stab.*, 2020, **171**, 1–9.

24 F. Tang and Y. G. Jeong, Improvement in thermal stability, elastic modulus, and impact strength of Poly(lactic acid) blends with modified polyketone, *Polymers*, 2022, **257**, 1–9.

25 B. Ma, H. Zhang, K. Wang, H. Xu, Y. He and X. Wang, Influence of scPLA microsphere on the crystallization behavior of PLLA/PDLA composites, *Compos. Commun.*, 2020, **21**, 1–6.

26 M. Guo, W. Wu, W. Wu and Q. Gao, Competitive Mechanism of Stereocomplexes and Homocrystals in High-Performance Symmetric and Asymmetric Poly(lactic acid) Enantiomers: Qualitative Methods, *ACS Omega*, 2022, **7**, 41412–41425.

27 Z. Gu, Y. Xu, Q. Lu, C. Han, R. Liu, Z. Zhou, T. Hao and Y. Nie, Stereocomplex formation in mixed polymers filled with two-dimensional nanofillers, *Phys. Chem. Chem. Phys.*, 2019, **21**, 6443–6452.

28 W. Li, Q. Ren, H. Zhu, M. Wu, Z. Weng, L. Wang and W. Zheng, Enhanced heat resistance and compression strength of microcellular poly (lactic acid) foam by promoted stereocomplex crystallization with added D-Mannitol, *J. CO₂ Util.*, 2022, **63**, 1–11.

29 J. Hirata, N. Kurokawa, M. Okano, A. Hotta and S. Watanabe, Evaluation of Crystallinity and Hydrogen Bond Formation in Stereocomplex Poly(lactic acid) Films by Terahertz Time-Domain Spectroscopy, *Macromolecules*, 2020, **53**, 7171–7177.

30 M. Guo, W. Wu, W. Wu, R. Wang, L. Huang and Q. Gao, Recent advances in enhancing stereocomplexation between poly(lactide) enantiomeric chains, *Phys. Chem. Chem. Phys.*, 2023, **25**, 17737–17758.

31 M. Fujita, T. Sawayanagi, H. Abe, T. Tanaka, T. Iwata, T. Ito, T. Fujisawa and M. Maeda, Stereocomplex formation through reorganization of poly(L-lactic acid) and poly(D-lactic acid) crystals, *Macromolecules*, 2008, **41**, 2852–2858.

32 B. Yu, L. Meng, S. Fu, Z. Zhao, Y. Liu, K. Wang and Q. Fu, Morphology and internal structure control over PLA microspheres by compounding PLLA and PDLA and effects on drug release behavior, *Colloids Surf., B*, 2018, **172**, 105–112.

33 L. Feng, X. Bian, G. Li and X. Chen, Compatibility and Thermal and Structural Properties of Poly(l -lactide)/Poly(l -Co- d -lactide) Blends, *Macromolecules*, 2022, **55**, 1709–1718.

34 S. Nouri, C. Dubois and P. G. Lafleur, Homocrystal and stereocomplex formation behavior of polylactides with different branched structures, *Polymers*, 2015, **67**, 227–239.

35 J. Sun, J. Shao, S. Huang, B. Zhang, G. Li, X. Wang and X. Chen, Thermostimulated crystallization of polylactide stereocomplex, *Mater. Lett.*, 2012, **89**, 169–171.

36 X. Jiang and L. Yang, Optothermal dynamics in whispering-gallery microresonators, *Light: Sci. Appl.*, 2020, **9**, 24.

37 A. R. Anwar, M. Mur and M. Humar, Microcavity- and Microlaser-Based Optical Barcoding: A Review of Encoding Techniques and Applications, *ACS Photonics*, 2023, **10**, 1202–1224.

38 T. N. Pham, S. Guerrault and C. Ayela, Polymer Microtip Based Fabry−Perot Interferometer for Water Content Determination in the Gas and Liquid Phase, *ACS Appl. Mater. Interfaces*, 2023, **15**, 46368–46378.

39 M. Loyez, M. Adolphson, J. Liao and L. Yang, From Whispering Gallery Mode Resonators to Biochemical Sensors, *ACS Sens.*, 2023, **8**, 2440–2470.

40 Y. C. Tao, X. D. Wang and L. S. Liao, Active whispering-gallery-mode optical microcavity based on self-assembled organic microspheres, *J. Mater. Chem. C*, 2019, **7**, 3443–3446.

41 G. C. Righini and S. Soria, Biosensing by WGM microspherical resonators, *Sensors*, 2016, **16**, 905.

42 N. Toropov, G. Cabello, M. P. Serrano, R. R. Gutha, M. Rafti and F. Vollmer, Review of biosensing with whispering-gallery mode lasers, *Light: Sci. Appl.*, 2021, **10**, 42.

43 S. H. Im, S. J. Park, Y. Jung, J. J. Chung and S. H. Kim, Strategy for Stereocomplexation of Polylactide Using O/W Emulsion Blending and Applications as Composite Fillers, Drug Carriers, and Self-Nucleating Agents, *ACS Sustainable Chem. Eng.*, 2020, **8**, 8752–8761.

44 L. Feng, X. Bian, G. Li and X. Chen, Thermal Properties and Structural Evolution of Poly(l -lactide)/Poly(d -lactide) Blends, *Macromolecules*, 2021, **54**, 10163–10176.

45 Y. Kong and J. N. Hay, The enthalpy of fusion and degree of crystallinity of polymers as measured by DSC, *Eur. Polym. J.*, 2003, **39**, 1721–1727.

46 B. Ma, H. Zhang, K. Wang, H. Xu, Y. He and X. Wang, Influence of scPLA microsphere on the crystallization behavior of PLLA/PDLA composites, *Compos. Commun.*, 2020, **21**, 1–6.

47 K. Tashiro, N. Kouno, H. Wang and H. Tsuji, Crystal Structure of Poly(lactic acid) Stereocomplex: Random Packing Model of PDLA and PLLA Chains As Studied by X-ray Diffraction Analysis, *Macromolecules*, 2017, **50**, 8048–8065.

48 Y. Yamamoto, Spherical resonators from π-conjugated polymers, *Polym. J.*, 2016, **48**, 1045–1050.

49 Y. Yamamoto, H. Yamagishi, J. S. Huang and A. Lorke, Molecular and Supramolecular Designs of Organic/Polymeric Micro-photoemitters for Advanced Optical and Laser Applications, *Acc. Chem. Res.*, 2023, **56**, 1469–1481.

50 Y. Yamamoto, S. Kushida, D. Okada, O. Oki, H. Yamagishi and Hendra, Self-Assembled π-Conjugated Organic/

Polymeric Microresonators and Microlasers, *Bull. Chem. Soc. Jpn.*, 2023, **96**, 702–710.

51 K. Tabata, D. Braam, S. Kushida, L. Tong, J. Kuwabara, T. Kanbara and Y. Yamamoto, Self-assembled conjugated polymer spheres as fluorescent microresonators, *Sci. Rep.*, 2014, **4**, 1–4.

52 D. Okada, T. Nakamura, D. Braam, T. D. Dao, S. Ishii, T. Nagao, A. Lorke, T. Nabeshima and Y. Yamamoto, Color-Tunable Resonant Photoluminescence and Cavity-Mediated Multistep Energy Transfer Cascade, *ACS Nano*, 2016, **10**, 7058–7063.

53 S. Kushida, D. Braam, T. D. Dao, H. Saito, K. Shibasaki, S. Ishii, T. Nagao, A. Saeki, J. Kuwabara, T. Kanbara, M. Kijima, A. Lorke and Y. Yamamoto, Conjugated Polymer Blend Microspheres for Efficient, Long-Range Light Energy Transfer, *ACS Nano*, 2016, **10**, 5543–5549.

54 M. Gao, C. Wei, X. Lin, Y. Liu, F. Hu and Y. S. Zhao, Controlled assembly of organic whispering gallery-mode microlasers as highly sensitive chemical vapor sensors, *Chem. Commun.*, 2017, **53**, 3102.

55 R. Vattikunta, D. Venkatakrishnarao, C. Sahoo, S. R. G. Naraharisetty, D. N. Rao, K. Mullen and R. Chandrasekar, Photonic Microresonators from Charge Transfer in Polymer Particles: Toward Enhanced and Tunable Two-Photon Emission, *ACS Appl. Mater. Interfaces*, 2018, **10**, 16723–16730.

56 D. Venkatakrishnarao, C. Sahoo, R. Vattikunta, M. Annadhasan, S. R. G. Naraharisetty and R. Chandrasekar, 2D Arrangement of Polymer Microsphere Photonic Cavities Doped with Novel N-Rich Carbon Quantum Dots Display Enhanced One- and Two-Photon Luminescence Driven by Optical Resonances, *Adv. Opt. Mater.*, 2017, **5**, 1700695.

57 M. Annadhasan, A. V. Kumar, D. Venkatakrishnarao, E. A. Mamonov and R. Chandrasekar, Mechanophotonics: precise selection, assembly and disassembly of polymer optical microcavities via mechanical manipulation for spectral engineering, *Nanoscale Adv.*, 2020, **2**, 5584.

58 R. Vattikunta, M. Annadhasan, R. Jada, M. D. Prasad, N. Mitetelo, K. Zhdanova, E. Mamonov, K. Müllen, T. Murzina and R. Chandrasekar, Multifunctional Chiral π-Conjugated Polymer Microspheres: Production and Confinement of NLO signal, Detection of Circularly Polarized Light, and Display of Laser-Triggered NLO Emission Shifts, *Adv. Opt. Mater.*, 2020, **8**, 2000431.

59 S. Kushida, D. Braam, C. Pan, T. D. Dao, K. Tabata, K. Sugiyasu, M. Takeuci, S. Ishii, T. Nagao, A. Lorke and Y. Yamamoto, Whispering Gallery Resonance from Self-Assembled Microspheres of Highly Fluorescent Isolated Conjugated Polymers, *Macromolecules*, 2015, **48**, 3928–3933.

60 W. Y. Heah, H. Yamagishi, K. Fujita, M. Sumitani, Y. Mikami, H. Yoshioka, Y. oki and Y. Yamamoto, Silk fibroin microspheres as optical resonators for wide-range humidity sensing and biodegradable lasers, *Mater. Chem. Front.*, 2021, **5**, 5653–5657.

61 N. Tanji, H. Yamagishi, K. Fujita and Y. Yamamoto, Nanoporous Fluorescent Microresonators for Non-wired Sensing of Volatile Organic Compounds down to the ppb Level, *ACS Appl. Polym. Mater.*, 2022, **4**, 1065–1070.

62 Hendra, A. Takeuchi, H. Yamagishi, O. Oki, M. Morimoto, M. Irie and Y. Yamamoto, Photochemically Switchable Interconnected Microcavities for All-Organic Optical Logic Gate, *Adv. Funct. Mater.*, 2021, **31**, 1–7.

63 Hendra, H. Yamagishi, W. Y. Heah, A. D. Malay, K. Numata and Y. Yamamoto, Micrometer-Scale Optical Web Made of Spider Dragline Fibers with Optical Gate Operations, *Adv. Opt. Mater.*, 2022, **11**, 2202563.

64 L. Cai, J. Pan, Y. Zhao, J. Wang and S. Xiao, Whispering gallery mode optical microresonators: Structures and sensing applications, *Phys. Status Solidi A*, 2020, **217**, 1900825.

65 O. Oki, S. Kushida, A. Mikosch, K. Hatanaka, Y. Takeda, S. Minakata, J. Kuwabara, T. Kanbara, T. D. Dao, S. Ishii, T. Nagao, A. Kuehne, F. Deschler, R. Friend and Y. Yamamoto, FRET-mediated near infrared whispering gallery modes: Studies on the relevance of intracavity energy transfer with Q-factors, *Mater. Chem. Front.*, 2018, **2**, 270–274.